THE JOURNAL OF BIOLOGICAL CHEMISTRY VOL. 284, NO. 43, pp. 29462–29469, October 23, 2009

A *cis*-Proline in α-Hemoglobin Stabilizing Protein Directs the Structural Reorganization of α-Hemoglobin*[S]

Received for publication, May 31, 2009, and in revised form, July 16, 2009 Published, JBC Papers in Press, August 25, 2009, DOI 10.1074/jbc.M109.027045

David A. Gell[‡1,2], Liang Feng[§1], Suiping Zhou[¶3], Philip D. Jeffrey[§], Katerina Bendak[‡], Andrew Gow[‖], Mitchell J. Weiss[¶], Yigong Shi[§4], and Joel P. Mackay[‡]

From the [‡]School of Molecular and Microbial Biosciences, University of Sydney, New South Wales 2006, Australia, the [§]Department of Molecular Biology, Lewis Thomas Laboratory, Princeton University, Princeton, New Jersey 08544, [¶]The Children's Hospital of Philadelphia and the University of Pennsylvania, Philadelphia, Pennsylvania 19104, and the [‖]Department of Pharmacology and Toxicology, Ernest Mario School of Pharmacy, Rutgers University, Piscataway, New Jersey 08854

α-Hemoglobin (αHb) stabilizing protein (AHSP) is expressed in erythropoietic tissues as an accessory factor in hemoglobin synthesis. AHSP forms a specific complex with αHb and suppresses the heme-catalyzed evolution of reactive oxygen species by converting αHb to a conformation in which the heme is coordinated at both axial positions by histidine side chains (bis-histidyl coordination). Currently, the detailed mechanism by which AHSP induces structural changes in αHb has not been determined. Here, we present x-ray crystallography, NMR spectroscopy, and mutagenesis data that identify, for the first time, the importance of an evolutionarily conserved proline, Pro[30], in loop 1 of AHSP. Mutation of Pro[30] to a variety of residue types results in reduced ability to convert αHb. In complex with αHb, AHSP Pro[30] adopts a *cis*-peptidyl conformation and makes contact with the N terminus of helix G in αHb. Mutations that stabilize the *cis*-peptidyl conformation of free AHSP, also enhance the αHb conversion activity. These findings suggest that AHSP loop 1 can transmit structural changes to the heme pocket of αHb, and, more generally, highlight the importance of *cis*-peptidyl prolyl residues in defining the conformation of regulatory protein loops.

Mammalian adult hemoglobin (HbA)[5] is a tetramer of two αHb and two βHb subunits, which is produced to extremely high concentrations (~340 mg/ml) in red blood cells. Numerous mechanisms exist to balance and coordinate HbA synthesis in normal erythropoiesis, and problems with the production of either HbA subunit give rise to thalassemia, a common cause of anemia worldwide. Previously, we identified α-hemoglobin stabilizing protein (AHSP) as an accessory factor in normal HbA production (1). AHSP forms a dimeric complex with αHb (see Fig. 1*A*) (2) but does not interact with βHb or HbA. AHSP also binds heme-free (apo) αHb (3) and may serve functions in both the folding of nascent αHb (4) and the detoxification of excess αHb that remains following HbA assembly (2, 5). Mice carrying an *Ahsp* gene knock-out display mild anemia, ineffective erythropoiesis, and enhanced sensitivity to oxidative stress (1, 6), features also observed in β-thalassemia patients due to the cytotoxic effects of free αHb.

Free αHb promotes the formation of harmful reactive oxygen species as a result of reduction/oxidation reactions involving the heme iron (7, 8). Reactive oxygen species can damage heme, αHb, and other cellular structures, resulting in hemoglobin precipitates and death of erythroid precursor cells (9–12). The presence of AHSP may explain how cells tolerate the slight excess of αHb that is observed in normal erythropoiesis, which is postulated to inhibit the formation of non-functional βHb tetramers, thus providing a robust mechanism for achieving the correct subunit stoichiometry during HbA assembly (13).

Structural and biochemical studies have begun to elucidate the molecular mechanism by which AHSP detoxifies αHb. AHSP binds to oxygenated αHb to generate an initial complex that retains the oxy-heme, as evidenced by a characteristic visible absorption spectrum (see Fig. 1*B*, *middle*) and resonance Raman spectrum (5). This initial oxy-αHb·AHSP complex then converts to a low spin Fe^{3+} complex (2), in which the heme iron is bound at both axial positions by the side chains of His^{58} and His^{87} from αHb (see Fig. 1*B*, *right*). The formation of this complex inhibits αHb peroxidase activity and heme loss (2). Bis-histidyl heme coordination is becoming increasingly recognized as a feature of numerous vertebrate and non-vertebrate globins (14) and has been shown previously to confer a relative stabilization of the Fe^{3+} over the Fe^{2+} oxidation state (15–17). Although bis-histidyl heme coordination has previously been detected in solutions of met-Hb, formed through spontaneous autoxidation of Hb (18–21), the bishis-αHb·AHSP complex provides the first evidence that the bis-histidyl heme may play a positive functional role in Hb biochemistry by inhibiting the production of harmful reactive oxygen species.

Despite its potential importance, the mechanism by which AHSP influences heme coordination in its binding partner is still unknown. As shown in Fig. 1*A*, AHSP binds αHb at a sur-

* This work was supported, in whole or in part, by National Institutes of Health Grants R01 DK61692 and R01 HL087427 (to M. J. W.). This work was also supported by grants from the Australian Research Council (to D. A. G. and J. P. M.).

[S] The on-line version of this article (available at http://www.jbc.org) contains supplemental Tables S1 and S2 and Figs. S1–S3.

The atomic coordinates and structure factors (code 3IA3) have been deposited in the Protein Data Bank, Research Collaboratory for Structural Bioinformatics, Rutgers University, New Brunswick, NJ (http://www.rcsb.org/).

[1] Both authors contributed equally to this work.

[2] To whom correspondence should be addressed. E-mail: dagell@mail.usyd.edu.au.

[3] Supported by a fellowship from the Cooley's Anemia Foundation.

[4] Supported by startup funds from Princeton University.

[5] The abbreviations used are: HbA, adult hemoglobin; αHb, α-subunit of hemoglobin; AHSP, αHb stabilizing protein; met-αHb, α-methemoglobin; AHSP-(P30A), AHSP carrying a proline to alanine substitution at position 30; MES, 4-morpholineethanesulfonic acid; PDB, Protein Data Bank; bishis, bis-histidyl; HQSC, heteronuclear single-quantum coherence.

face away from the heme pocket, and thus structural changes must somehow be transmitted through the αHb protein. It is intriguing that the free AHSP protein switches between two alternative conformations linked to *cis*/*trans* isomerization of the Asp^{29}-Pro^{30} peptide bond in loop 1 (22) and that, in complex with αHb, this loop is located at the αHb·AHSP interface (see Fig. 1*A*). Peptide bonds preceding proline residues are unique in that the *cis* or *trans* bonding conformations have relatively similar stabilities (23), allowing an interconversion between these conformations that can be important for protein function (24, 25). Previous x-ray crystal structures of αHb·AHSP complexes have been obtained only with a P30A mutant of AHSP, in which isomerization is abolished and the Asp^{29}-Ala^{30} peptide bond adopts a *trans* conformation, leaving the potential structural and functional significance of the evolutionarily conserved Pro^{30} undisclosed. Here, we demonstrate a functional role for AHSP Pro^{30} in conversion of oxy-αHb to the bis-histidyl form and identify a specific structural role for a *cis* Asp^{29}-Pro^{30} peptide bond in this process. From a mechanistic understanding of how AHSP promotes formation of bis-histidyl αHb, we may eventually be able to engineer AHSP function as a tool in new treatments for Hb diseases such as β-thalassemia.

EXPERIMENTAL PROCEDURES

Protein Production—Full-length human AHSP (102 residues), and a construct with the C-terminal unstructured residues deleted (AHSP residues 1–90; AHSP-(1–90), were expressed in *Escherichia coli* BL21 and purified as described previously (3). The final purified proteins contained an additional Gly-Ser at the N terminus as a consequence of the expression system. αHb from human blood was purified as described previously (3). Isotopic labeling of ASHP was achieved by expression in shaker flasks with $^{15}NH_4Cl$ and ^{13}C-glucose as sole nitrogen and carbon sources (26). Met-αHb was prepared from oxy-αHb by oxidation with 5 molar eq of $K_3Fe(CN)_6$ and filtered over Sephadex G-25 (Amersham Biosciences).

NMR Spectroscopy—AHSP and αHb·AHSP complexes were prepared at ~1 mM concentration in 10–20 mM Na_2HPO_4/NaH_2PO_4, pH 6.9 (95% ^1H_2O and 5% ^2H_2O) and 2 μM 5,5-dimethylsilapentanesulfonate. Data were collected at 288 K (AHSP-(1–90)), 298 K (AHSP) and 303 K (αHb·AHSP complexes) on Bruker Avance 600 and 800 MHz spectrometers, processed in TOPSPIN (Bruker), and analyzed using SPARKY.[6] Backbone assignments were obtained using standard triple-resonance solution NMR methods (27). Side chain ^{13}C assignments were made from the CC(CO)NH experiment (28). The ratio of the *cis*/*trans* Xaa^{29}-Pro^{30} peptide bond isomers was determined from ^{15}N-HSQC peak volumes.

X-ray Crystallography—A complex between oxy-αHb and AHSP residues 1–91 (AHSP-(1–91)) was produced as described (5) and oxidized by 4 molar eq of $K_3Fe(CN)_6$. Crystals were grown at 4 °C using the hanging drop vapor diffusion method. The well buffer contains 0.1 M MES, pH 6.5, 4% acetonitrile, and 14.5% (w/v) PEG3000. The crystals, with a typical dimension of 0.05 × 0.05 × 0.1 mm^3, belong to the space group $P6_122$ and contain two complexes per asymmetric unit. The unit cell has a dimension of $a = b = 65.23$ Å and $c = 439.66$ Å. Crystals were equilibrated in buffer containing 0.1 M MES, pH 6.5, 15% (w/v) PEG3000, and 21% (v/v) glycerol, and were flash frozen under a cold nitrogen stream. The native data sets were collected at the National Synchrotron Light Source X25 at the Brookhaven National Laboratories. The data were processed with Denzo and Scalepack (29). The structure was solved by molecular replacement using AMoRe (30). The atomic models of AHSP and αHb were built using O (31) and refined using CNS (32). The final refined atomic model, at 3.2 Å resolution, contains residues 1–91 of AHSP and residues 2–136 of αHb.

Isothermal Titration Calorimetry—Isothermal titration calorimetry was carried out on a MicroCal VP-ITC instrument in 20 mM sodium phosphate (pH 7.0) at 20 °C. Oxy-αHb, CO-αHb, or met-αHb (40–100 μM) was injected into AHSP (4–10 μM). Sucrose (0.45 M) was included in all buffers for titrations of met-αHb to inhibit precipitation. AHSP·αHb binding curves produced good fits to a simple 1:1 binding model using a non-linear least squares algorithm (supplemental Fig. S1).

Measurements of Oxy-αHb Conversion Rates—Conversion of αHb (10 μM) to bishis-αHb was measured by UV-visible absorption spectroscopy at 30 °C in the presence of a 1.2 molar excess of AHSP in 20 mM sodium phosphate, pH 7.0, with 10 μM diethylenetriaminepenta-acetic acid. After confirming the presence of isosbestic points in the spectra at 529 and 592 nm, the conversion rates were calculated by fitting the change in absorbance at 576 nm to a three-parameter exponential function.

RESULTS

Mutation of Pro^{30} Inhibits the Conversion of Oxy-αHb to Bishis-αHb—To investigate the function of Pro^{30} in AHSP, we generated a number of point mutants at this position and assayed their ability to convert oxy-αHb to the protective bis-histidyl form. As shown in Fig. 1*B*, the oxy-αHb·AHSP and bishis-αHb·AHSP complexes display characteristic visible absorption spectra that allow the conversion process to be conveniently monitored. A series of representative spectra obtained during conversion of oxy-αHb·AHSP are shown in Fig. 2*A*. Each spectrum can be fit as a sum of the pure oxy- and bishis-αHb·AHSP spectra, and the series displays isosbestic points at 529 and 592 nm. The change in absorbance at 576 nm was fit to a single exponential function (Fig. 2*B*, *closed circles*) to obtain a rate constant. In comparison to the oxy-αHb·AHSP complex, the spectra of oxy-αHb alone displayed only a minor change at 576 nm (Fig. 2*B*, *open squares*) and lacked the isosbestic points at 529 and 592 nm, indicating a process distinct from conversion to bis-histidyl αHb (precipitation was evident).

Upon mutation of Pro^{30} to any of the residues Ala, Phe, Gly, Val, or Trp, we observed a ~4-fold reduction in the rate constant ($p < 0.001$) (Table 1 and Fig. 2*C*, *lanes 5–9*). The same isosbestic points were observed in each reaction. In contrast, alanine mutations introduced at positions 29 or 31 had minor effects (Fig. 2*C*). These results indicate that efficient conversion

[6] T. D. Goddard and D. G. Kneller, SPARKY 3, University of California, San Francisco.

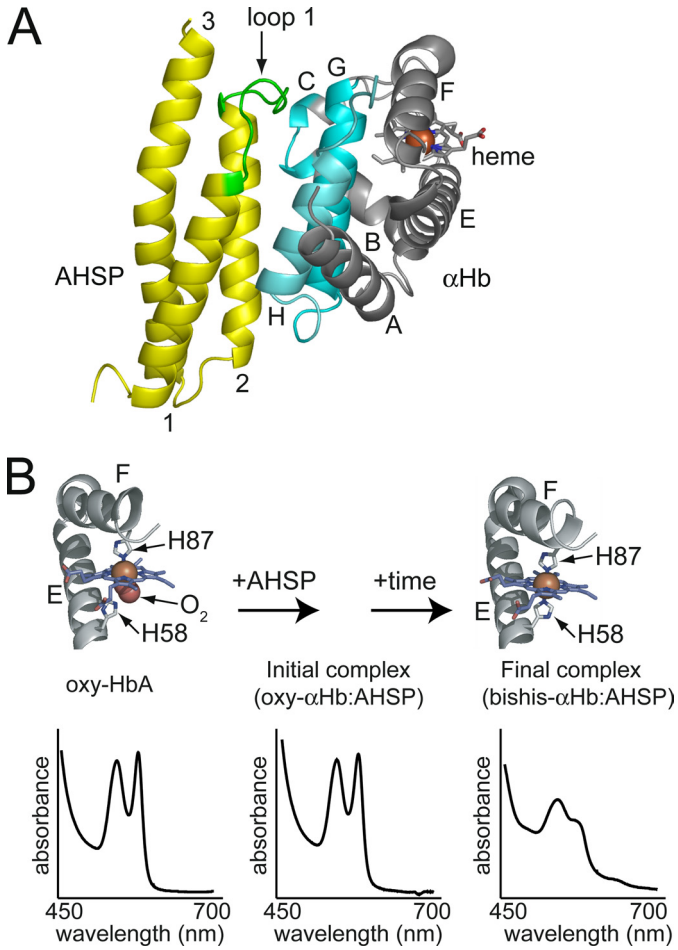

FIGURE 1. **Summary of αHb·AHSP interactions.** *A*, the αHb·AHSP complex(PDB code 1Z8U) (2). The interface is formed from helices 1 and 2 and the intervening loop 1 (*green*) of AHSP, together with helices G-H and the B-C corner of αHb (*cyan*). *B*, detailed views of the heme binding site of αHb as it appears in oxy-HbA (PDB code 1GZX) (69) and the final bis-histidyl αHb·AHSP complex (PDB code 1Z8U) with two histidine ligands to the iron. Typical visible absorption spectra in the region 450–700 nm are shown.

of oxy-αHb is dependent on properties of the Pro^{30} residue that cannot be substituted by other residue types.

Isothermal titration calorimetry revealed that most of the Pro^{30} mutants bound αHb more tightly than wild-type AHSP (Table 1), demonstrating that reduction in the αHb conversion rate did not correlate with the affinity of AHSP for αHb. These data suggest that Pro^{30} causes a comparative destabilization of the initial oxy-αHb·AHSP complex, while also lowering the activation barrier for conversion to bishis-αHb·AHSP.

We also determined the affinity of wild-type AHSP or mutant AHSP-(P30A) for met-αHb, a pre-oxidized form of free αHb. We have previously shown that met-αHb reacts with AHSP to rapidly form bishis-αHb·AHSP, apparently without the formation of an intermediate complex (5). We found that the affinity of met-αHb for AHSP and AHSP-(P30A) is very similar (K_D = 4.3 and 5.0 nM, respectively) (supplemental Fig. S1), indicating that Pro^{30} does not significantly influence the thermodynamic stability of the final bis-histidyl complex.

The cis/trans Conformation of the Peptide Bond between Residues 29 and 30 of AHSP Correlates with Ability to Convert Oxy-αHb to the Bis-histidyl Form—Introduction of the P30A mutation abrogates the *cis*/*trans* isomerization of AHSP, resulting in a *trans* Asp^{29}-Ala^{30} peptide bond (5, 22). The remaining Pro^{30} mutants also adopt a single conformation, assumed to be *trans* (as judged by one-dimensional NMR; data not shown), and all display a similar 4-fold reduction in activity. Prolyl *cis*/*trans* isomerization is known to modulate the function of numerous proteins (24, 25), raising the possibility that the *cis*/*trans* conformation of the Asp^{29}-Pro^{30} peptide bond might be important for AHSP function. To investigate this hypothesis, we made substitutions to amino acids surrounding Pro^{30}. Previous work on peptides (33, 34) and proteins (35, 36) has established that the ratio of *cis* to *trans* prolyl conformers is strongly influenced by the identity of the preceding residue.

We found that D29F and D29W mutations resulted in enhanced αHb conversion activity compared with wild-type AHSP (Fig. 2*C*). In contrast, D29A, L31A, and L31W mutations in AHSP had little effect on the αHb conversion rate. To control for effects of the D29W mutation that might be unrelated to its influence on the conformation of the Xaa^{29}-Xaa^{30} peptide bond, we generated a double mutant, D29W,P30A. Significantly, this mutant had the same low activity as AHSP-(P30A) (Fig. 2*C*, *lane 12*), confirming that the stimulating effect of the D29W mutation relies upon the presence of Pro^{30}.

To investigate the structural consequences of these mutations, we assigned backbone ^{15}N, H_N, and $^{13}C_\alpha$ resonances for the D29A, D29F, D29W, L31A, and L31W mutants. All mutants displayed evidence of distinct *cis*/*trans* isomers (supplemental Fig. S2). To assign these isomers, we used proline side chain carbon resonances. The chemical shift difference $\delta(^{13}C_\beta)$-$\delta(^{13}C_\gamma)$ for proline is diagnostic for the conformation of the preceding peptide bond, with average values of 4.5 ± 1.2 and 9.6 ± 1.3 ppm (±1 S.D.) observed for *trans* and *cis* isomers, respectively (37). The relative abundances of the *cis* and *trans* isomers were then calculated from ^{15}N-HSQC peak volumes. Overall, there was positive correlation between the fraction of *cis* peptide in free AHSP and the conversion rate of the corresponding oxy-αHb·AHSP complex (Fig. 2*D*).

The Conformation of AHSP Is the Same in Oxy-αHb and Bishis-αHb Complexes—To gain insight into the function of AHSP Pro^{30} in oxy-αHb conversion, we carried out structural analyses of the initial oxy-αHb·AHSP and final bishis-αHb·AHSP complexes. Although free AHSP exists as a mixture of two conformers, only a single conformer can be detected in complex with αHb by NMR methods (5, 22). Using a construct of AHSP in which the C-terminal unstructured residues were deleted (AHSP residues 1–90; AHSP-(1–90)), we could obtain complete backbone and proline side chain carbon assignments in a complex with αHb. We confirmed that AHSP-(1–90), and mutants thereof, showed the same pattern of activity and conformational preference as the full-length proteins (Table 1 and Fig. 2, *C* and *D*).

To prevent conversion of the initial αHb·AHSP complex to the bis-histidyl complex, we used carbonmonoxy-αHb (CO-αHb) in the place of oxy-αHb. Importantly, the ^{15}N-HSQC spectra of CO-αHb·AHSP-(1–90) and oxy-αHb·AHSP-(1–90) are essentially identical (supplemental Fig. S3). The chemical shift difference $\delta(^{13}C_\beta)$-$\delta(^{13}C_\gamma)$ for Pro^{30} in the

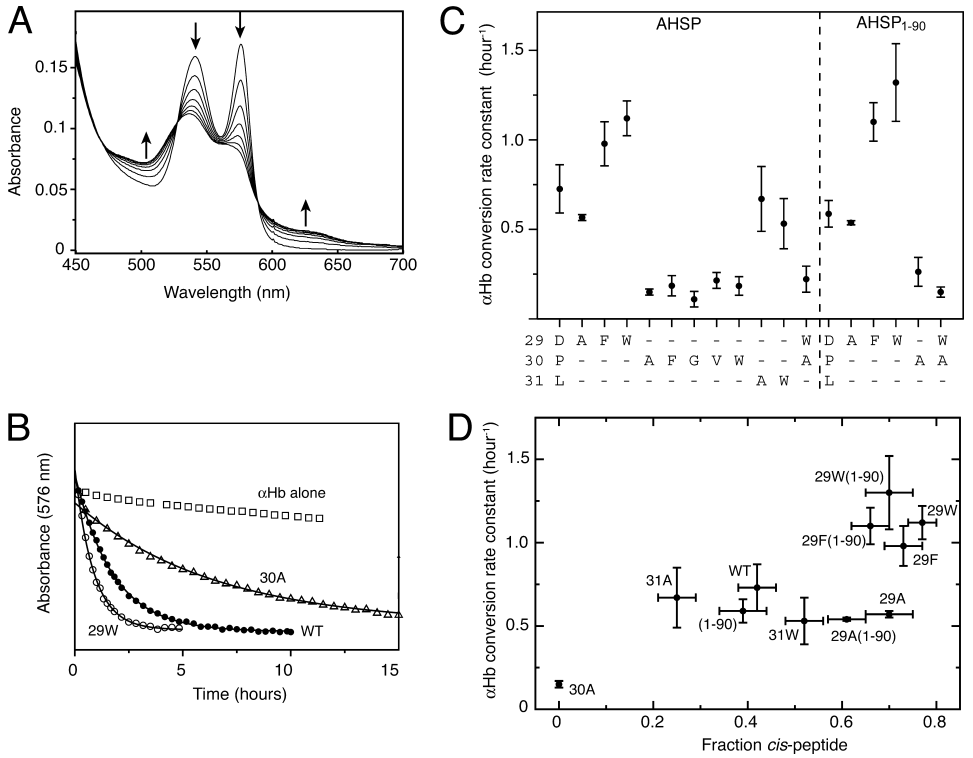

FIGURE 2. **Oxy-αHb conversion rates for AHSP loop mutants.** *A*, visible absorption spectra (450–700 nm) obtained over a typical oxy-αHb·AHSP to bishis-αHb·AHSP conversion time course (directions of spectral changes are indicated by *arrows*). *B*, time courses of absorbance at 576 nm for oxy-αHb alone (*squares*), the oxy-αHb·AHSP complex (*filled circles*), and complexes containing P30A (*triangles*) or D29W (*open circles*) mutants of AHSP. Fits to single exponential functions are shown (*solid lines*). *C*, summary of oxy-αHb conversion rate data obtained for AHSP and AHSP-(1–90) carrying various mutations at positions Asp^{29}, Pro^{30}, Leu^{31}, and the double mutant D29W,P30A (*error bars* represent ±1 S.D.; further details are provided in Table 1). *D*, a correlation was observed between the fraction of AHSP present in the *cis* Xaa^{29}-Xaa^{30} peptidyl conformation and the αHb conversion rate constant (correlation coefficient $r = 0.75$; $p < 0.01$). *WT*, wild-type.

TABLE 1
αHb·AHSP interaction parameters

AHSP sequence	Affinity constant (K_D)[a]	Oxy-αHb conversion rate constant[b]	Proportion of *cis* Xaa^{29}–Xaa^{30} peptide
	nM	h^{-1}	
Wild-type AHSP	98 ± 10	0.73 ± 0.14 (n = 12)	0.42 ± 0.04[c]
P30A	33 ± 3.0	0.15 ± 0.02 (n = 6)	0[d]
P30G	450 ± 60	0.11 ± 0.04 (n = 4)	0
P30V	42 ± 7.0	0.22 ± 0.04 (n = 4)	0
P30F	15 ± 2.9	0.19 ± 0.06 (n = 6)	0
P30W	7.7 ± 2.3	0.18 ± 0.05 (n = 5)	0
D29A	250 ± 30	0.57 ± 0.02 (n = 5)	0.70 ± 0.05
D29F		0.98 ± 0.12 (n = 5)	0.73 ± 0.04
D29W	53 ± 4.2	1.12 ± 0.10 (n = 5)	0.77 ± 0.03
L31A		0.67 ± 0.18 (n = 5)	0.25 ± 0.04
L31W		0.53 ± 0.14 (n = 5)	0.52 ± 0.04
D29W,P30A		0.22 ± 0.07 (n = 5)	0
AHSP-(1–90)	93 ± 5	0.59 ± 0.07 (n = 9)	0.39 ± 0.05
P30A-(1–90)		0.26 ± 0.08 (n = 3)	0
D29A-(1–90)		0.54 ± 0.01 (n = 3)	0.61 ± 0.04
D29F-(1–90)		1.1 ± 0.11 (n = 4)	0.66 ± 0.04
D29W-(1–90)		1.3 ± 0.22 (n = 5)	0.70 ± 0.05
D29W,P30A-(1–90)		0.15 ± 0.03 (n = 2)	0

[a] Values from single isothermal titration calorimetry experiments, with fitting errors for unweighted non-linear least squares regression analysis using MicroCal Origin software. Representative data are shown in supplemental Fig. S1. AHSP binding to oxy- or CO-αHb yielded identical K_D within the bounds of experimental error (supplemental Table S1).
[b] Determined from UV-visible absorption spectroscopy at 30 °C. The mean and S.D. for n independent measurements are reported.
[c] Calculated from ^{15}N-HSQC peak volumes at 25 °C: a mean value (± 1 S.D.) for all residues where amide signals from both the *cis* and *trans* Xaa^{29}-Pro^{30} isomers can be resolved. Data from two independently prepared samples were combined.
[d] P30*X* mutants adopted a single conformer in the basis of one-dimensional NMR.

CO-αHb·AHSP-(1–90) complex was 9.3 ppm, indicating a *cis* Asp^{29}-Pro^{30} conformation. In comparison, Pro^{60} and Pro^{80} yield values of 3.7 and 2.6 ppm, respectively, and are thus predicted to be in the *trans*-peptidyl conformation, consistent with our previous crystal structures (2, 5). A comparison of backbone chemical shifts between AHSP-(1–90) and AHSP-(1–90, P30A), both in complex with CO-αHb, reveals substantial differences in the conformation of loop 1 (Fig. 3*A*), consistent with the presence of a *cis* Asp^{29}-Pro^{30} peptide bond in CO-αHb·AHSP-(1–90).

To determine whether AHSP undergoes any conformation changes concomitant with αHb conversion, we incubated unlabeled oxy-αHb with ^{15}N-labeled AHSP-(1–90) at 30 °C and recorded ^{15}N-HSQC spectra at 22-min intervals for 18 h. The evolution of the final bishis-αHb·AHSP complex was confirmed by UV-visible spectroscopy. Only small changes in the ^{15}N-HSQC spectra were observed in this experiment (Fig. 3*B*, *bars*), indicating only minor changes in AHSP structure. These changes were much less pronounced than the differences between the *cis*/*trans* conformers of free AHSP-(1–90) (Fig. 3*B*, *dashed line*) or between the *cis* and *trans* conformations of AHSP-(1–90) and AHSP-(1–90,P30A) bound to CO-αHb (Fig. 3*A*). Backbone chemical shifts were also assigned for AHSP-(1–90,P30A), for which peptide bond isomerization has been shown not to occur (2, 5), in complex with CO-αHb and bishis-αHb. Small chemical shift differences were observed, and these were similar to those observed for AHSP-(1–90). Together, these data reveal that the structure of AHSP changes very little during αHb conversion, and that, in wild-type AHSP complexes, the Asp^{29}-Pro^{30} peptide bond is likely to remain in a *cis* conformation throughout.

Crystal Structure of Wild-type bishis-αHb·AHSP Complex—To understand in more detail the influence of *cis*-peptidyl Pro^{30} on the structure and function of αHb·AHSP complexes, we turned to x-ray crystallography. Despite extensive efforts over three years, we were unable to produce crystals of oxy-αHb complexed with wild-type human AHSP. Finally, after screening ~8,000 different conditions, we eventually generated small crystals of bishis-αHb·AHSP-(1–91). The structure of this complex was determined by molecular replacement and refined to a 3.2 Å resolution (Fig. 4 and supplemental Table S2).

Aside from loop 1 of AHSP, the conformations of individual subunits within the bishis-αHb·AHSP-(1–91) complex are vir-

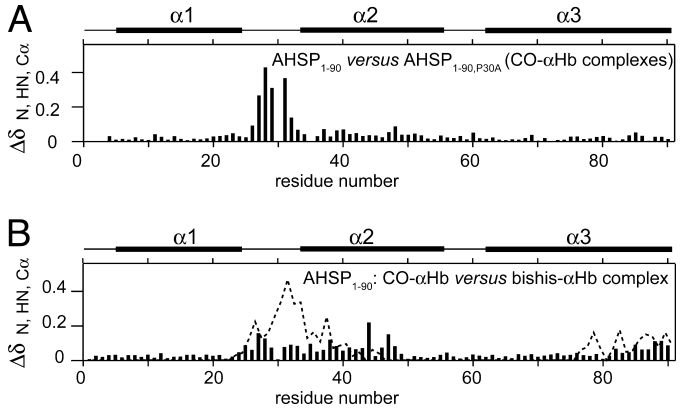

FIGURE 3. **AHSP-(1–90) contains a *cis* Asp^{29}-Pro^{30} peptide bond in complex with CO-αHb and bishis-αHb.** *A*, mean weighted chemical shift differences (^{15}N, H_N, and $^{13}C_\alpha$ nuclei; $\Delta\delta_{N,HN,C\alpha}$) between AHSP-(1–90) and AHSP-(1–90,P30A) in their respective complexes with CO-αHb. Structural differences are limited to the Pro^{30} loop. *B*, mean weighted chemical shift changes for residues in AHSP upon conversion from the CO-αHb·AHSP-(1–90) complex to the bishis-αHb·AHSP-(1–90) complex (*bars*). Shift changes in the Pro^{30} loop are small compared with the differences between the *cis* and *trans* Asp^{29}-Pro^{30} isomers of free AHSP-(1–90) (*dashed line*).

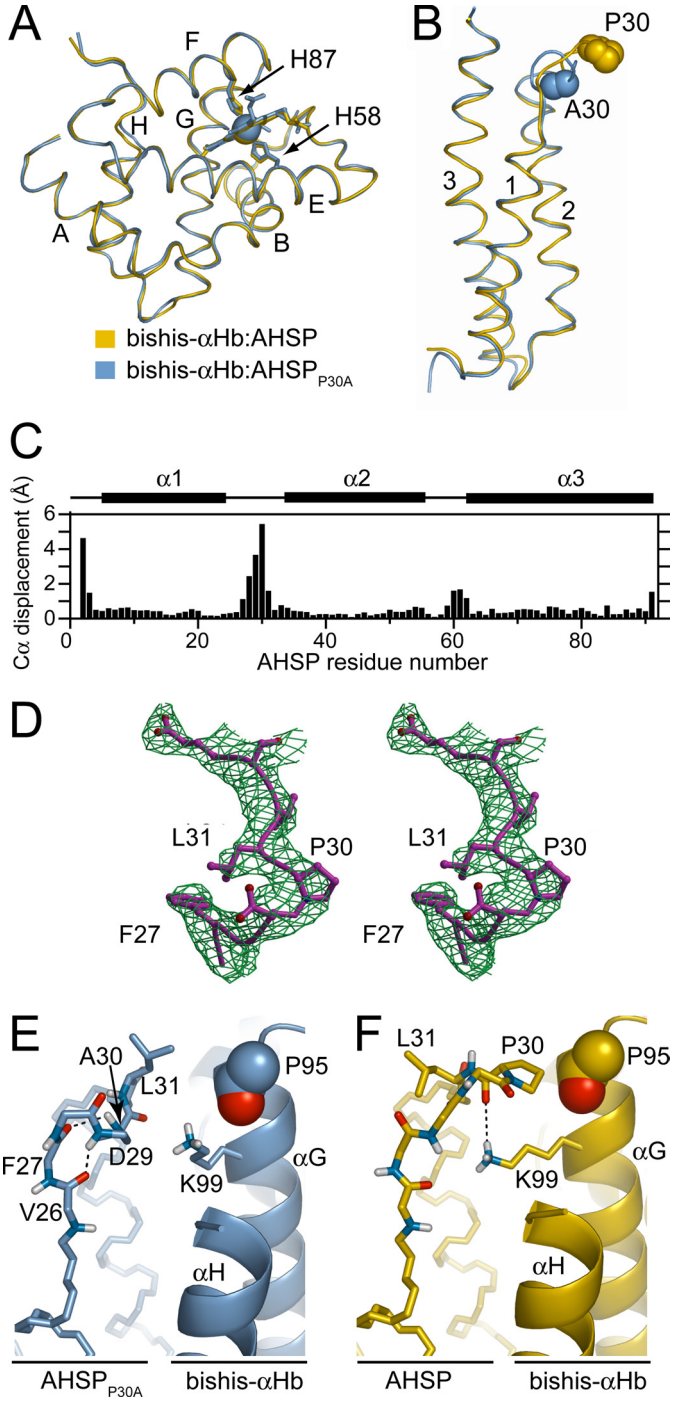

FIGURE 4. **Structural features of the wild-type bishis-αHb[chemp]AHSP-(1–91) complex.** Backbone overlays of the individual subunits of the bishis-αHb·AHSP-(1–91) (*yellow*; PDB code 3IA3) and bishis-αHb·AHSP-(1–91,P30A) (*blue*; PDB code 1Z8U) complexes showing αHb subunits (root mean square deviation of 0.4 Å over 135 aligned backbone C_α atoms) with conserved bis-histidyl heme coordination (*A*) and AHSP-(1–91) with Ala^{30} and Pro^{30} side chains shown in space-fill (*B*). *C*, plot of the distance between C_α positions for the AHSP alignment shown in *B*. *D*, stereo view of the *cis* Asp^{29}-Pro^{30} conformation of the Pro^{30} loop in the bishis-αHb·AHSP-(1–91) complex. The electron density $2F_o - F_c$ map, contoured at 1.0 σ, is shown in *green*. *E*, detail of the bishis-αHb·AHSP-(1–91,P30A) complex showing intramolecular backbone hydrogen bonding in the loop. *F*, detail of the bishis-αHb·AHSP-(1–91) complex showing the Pro^{30} side chain positioned close to the backbone of Pro^{95} (*spheres*) in helix G of αHb (*αG*).

tually identical to their counterparts in our previously determined structure of bishis-αHb·AHSP-(1–91,P30A) (Fig. 4), and the interaction interface comprises the same network of van der Waals interactions and hydrogen bonds as described for the earlier structure (2).

In contrast, a marked difference is observed in the organization of AHSP loop 1 in the two bis-histidyl complexes (Fig. 4, *B* and *C*) that mirrors our NMR findings for the CO-αHb complexes (Fig. 3*A*). The x-ray structure confirms the existence of a *cis* Asp^{29}-Pro^{30} amide bond in AHSP (Fig. 4*D*) and reveals the significant effect of this bond on the molecular structure of loop 1. In bishis-αHb·AHSP-(1–91,P30A) the backbone amides of loop 1 residues Asp^{29} and Ala^{30} form hydrogen bonds with the backbone carbonyls of Val^{26} and Phe^{27}, respectively, giving rise to a single helical turn in AHSP loop 1 (Fig. 4*E*). The same hydrogen-bonding pattern is precluded in the wild-type AHSP because proline lacks an amide proton. Instead, the Pro^{30} loop projects out further toward αHb (Fig. 4*F*). In this position, the carbonyl of Pro^{30} forms a hydrogen bond with the Lys^{99} side chain of helix G in αHb, and the Pro^{30} side chain makes van der Waals contacts with the backbone of Pro^{95} in helix G. The Ala^{30} side chain faces away from αHb and makes no contacts with αHb. Thus, the distinguishing feature of the wild-type bishis-αHb·AHSP interface, which could not be inferred from prior crystallography studies, is the packing of the rigid Pro^{30} side chain against helix G of αHb.

DISCUSSION

Recently, we obtained the first evidence that bis-histidyl heme coordination may have a positive functional role in detoxification of αHb, by inhibiting the production of harmful reactive oxygen species (2). Defining the role of bis-histidyl heme coordination in erythroid biology should also provide insights into the functional properties of bis-histidyl heme structures in other systems, such as the hemoglobins of some arctic fish species (38) and other mammalian globins such as neuroglobin and cytoglobin (39). Ultimately, understanding how and why AHSP promotes formation of bis-histidyl αHb may allow us to design experimental strategies to modify AHSP function in new treatments for thalassemia (40).

Our current findings indicate that loop 1 of AHSP plays an important role in the transmission of structural changes to the heme pocket of αHb. A *cis* Asp^{29}-Pro^{30} bond is an important structural and functional feature of AHSP in complex with αHb. This conclusion was not evident from previous studies, which were expedited by the favorable effects of a P30A mutation upon crystallization.

The Mechanism of oxy-αHb Conversion—Conversion of oxy-αHb to the bis-histidyl conformation involves a significant reorganization of the αHb subunit, an rms shift of 3.2 Å over 135 C_α atoms compared with HbA (2). Despite this, we find that AHSP retains a remarkably similar conformation throughout the conversion process, making it unlikely that the reorganization of the αHb subunit is driven by a conformational change in AHSP. Rather, we liken the initial binding of AHSP to oxy-αHb to the setting of a "molecular mousetrap" in which some type of strain is introduced into the structure of oxy-αHb that is subsequently released in a structural rearrangement of the αHb subunit alone. Several lines of evidence suggest that this rearrangement is coupled with autoxidation of the heme iron. First, AHSP can bind to deoxy-αHb but cannot convert the Fe^{2+} heme to a bis-histidyl structure (41, 42). A preference for Fe^{3+} over Fe^{2+} has previously been observed in other bis-histidyl heme proteins (15–17). Second, conversion of Fe^{3+} met-αHb, which at physiological pH contains only a weakly bound water molecule in the distal heme pocket, occurs simultaneously with (or very rapidly after) binding to AHSP, suggesting that dissociation of superoxide is the rate-limiting step in the conversion of oxy-αHb·AHSP.

In the mousetrap mechanism, the function of AHSP appears to be 2-fold: to enhance the rate of heme autoxidation and to reduce the barrier to bishistidyl coordination imposed by the protein matrix. Presumably, the key to understanding how AHSP potentiates autoxidation lies in the structure of the initial oxy-αHb·AHSP complex. Although we have been unsuccessful in attempts to crystallize this complex, we have been able to obtain an x-ray crystal structure of the AHSP-(1–91,P30A) mutant bound to oxy-αHb (5), possibly because of the slow conversion of the P30A mutant complex at 4 °C. The presence of a detergent molecule in the heme pocket warrants some caution in interpreting this structure. Nevertheless, it provides a fortuitous opportunity to gain possible insights into the AHSP mechanism. Strikingly, the F-helix of αHb, which carries the proximal His^{87} in native αHb, is disordered in this crystal. A predicted increase in hydration of the heme (43), and/or a greater mobility of the heme-pocket histidines (18, 44) are plausible explanations for the comparatively rapid autoxidation of the oxy-αHb·AHSP complex. By way of comparison, it is known that even relatively minor changes in the heme pocket structure can have significant effects on the stability of oxy-heme. For example, an Mb mutant with the side chains of His^{64} and Val^{68} interchanged adopts a bis-histidyl heme coordination geometry and undergoes very rapid autoxidation in the presence of oxygen (45).

The current study suggests one mechanism by which AHSP may destabilize the oxy-αHb structure. In bishis-αHb·AHSP, the Pro^{30} side chain makes contact with helix G of αHb, and NMR data indicate that a similar conformation of the Pro^{30} loop is present in the initial oxy-αHb·AHSP complex. Mutation and thermodynamic data indicate that Pro^{30} destabilizes the oxy- but not the bishis-αHb·AHSP complex, leading to the hypothesis that Pro^{30} introduces a steric clash with the N terminus of helix G in oxy-αHb. Such an interaction might be one factor promoting a strained mousetrap conformation in αHb. Indeed, comparison of the oxy-αHb·AHSP-(1–91,P30A) and bishis-αHb·AHSP-(1–91) crystal structures shows that the Pro^{30} loop conformation could not be accommodated in the former structure without some displacement of helix G. Distortion of helix G in αHb is a plausible route through which AHSP might disrupt the structure of the adjacent F-helix and consequently the heme pocket. Clearly AHSP-(P30A) retains some ability to stabilize bishis-αHb indicating that additional contacts must also be involved.

In the αHb·AHSP complex, bonding of a second histidine side chain to the ferric heme iron stabilizes a switch in the conformation of αHb to a less redox active state. Mousetrap models have been invoked to describe other systems in which a transition between two alternate protein conformations is triggered in response to a highly localized bond rearrangement (46–48). The serpin class of serine protease inhibitors is one notable example. Cleavage of a serpin by its targeted protease triggers a large conformational change that traps the protease in an irreversible complex (46).

Evolutionary Conservation of Pro^{30}—The importance of Pro^{30} for AHSP function is highlighted by its conservation across species. Interestingly, AHSP from the South American opossum *Monodelphis domestica* is one of the very few AHSP sequences to lack a proline residue in loop 1. The opossum αHb sequence is also highly unusual in lacking a distal histidine, precluding the adoption of bis-histidyl coordination geometry and providing indirect support for the hypothesis that Pro^{30} is present to optimize the formation of the bis-histidyl complex. In addition to sequestering and detoxifying excess αHb, mouse knock-out studies suggest that AHSP may also function as an αHb-specific chaperone during Hb folding (4). The function of AHSP *in vivo* might well involve a subtle balance between these activities, and it may be that Pro^{30} has been adopted during evolution to optimize the rate of free αHb conversion. Such relatively small changes in protein activity can be highly significant at the level of cell and organism function. A familiar example is haploinsufficiency, in which inheritance of one defective allele reduces the expression of the respective protein ~2-fold and results in disease (49).

A Stable cis-Peptidyl Proline Motif That Defines an Active Loop Conformation—Proline residues are unique in that the *cis* or *trans* conformations of a preceding peptide bond have relatively similar stabilities (23). Interconversion between these conformations can influence protein folding (50) and function (24, 25). Alternatively, our results indicate that a stable *cis* peptide bond can confer important structural and functional properties, in this case driving a conformational change in a partner protein.

The cyclic structure of proline restricts the phi backbone dihedral angle, and, consequently, proline residues are associated with restricting protein loop mobility (51–53). Furthermore, a *cis* Xaa-Pro bond introduces more severe steric con-

straints on ϕ and ψ backbone angles than occurs for *trans* Xaa-Pro bonds (54). Consequently, *cis* and *trans* Xaa-Pro motifs have distinct structural preferences: a survey of the PDB reveals that *cis* Xaa-Pro is most commonly found in bend structures (regions where the backbone changes direction by $>70^\circ$ in the absence of backbone hydrogen bonding) (55) and least likely to appear in helical conformations (56). In addition, the lack of an amide proton means that proline cannot act as a hydrogen bond donor to stabilize regular secondary structure. Accordingly, loop 1 in bishis-αHb·AHSP crystal structure contains a bend that is replaced by a helical segment in the bishis-αHb·AHSP-(P30A) structure. This helical turn compacts loop 1 and prevents contact with helix G of αHb.

Cis Xaa-Pro motifs have been found to play precise structural roles in several protein folds (57–59), active sites (60–65) and protein interaction surfaces (66–68). Here we provide structural data to show that, within the αHb·AHSP complex, the *cis* Asp^{29}-Pro^{30} motif introduces intersubunit contacts that potentiate autoxidation of oxy-αHb. We envisage that *cis*-peptidyl proline may play a general role in defining the structure of regulatory protein loops.

Acknowledgments—We thank Bill Bubb and Chris Blake for expert maintenance of the 600-MHz NMR spectrometer in Sydney and the 800-MHz spectrometer in Canberra and M. Becker and A. Sexana at Brookhaven National Laboratory National Synchrotron Light Source beamlines for help.

REFERENCES

1. Kihm, A. J., Kong, Y., Hong, W., Russell, J. E., Rouda, S., Adachi, K., Simon, M. C., Blobel, G. A., and Weiss, M. J. (2002) *Nature* **417,** 758–763
2. Feng, L., Zhou, S., Gu, L., Gell, D. A., Mackay, J. P., Weiss, M. J., Gow, A. J., and Shi, Y. (2005) *Nature* **435,** 697–701
3. Gell, D., Kong, Y., Eaton, S. A., Weiss, M. J., and Mackay, J. P. (2002) *J. Biol. Chem.* **277,** 40602–40609
4. Yu, X., Kong, Y., Dore, L. C., Abdulmalik, O., Katein, A. M., Zhou, S., Choi, J. K., Gell, D., Mackay, J. P., Gow, A. J., and Weiss, M. J. (2007) *J. Clin. Invest.* **117,** 1856–1865
5. Feng, L., Gell, D. A., Zhou, S., Gu, L., Kong, Y., Li, J., Hu, M., Yan, N., Lee, C., Rich, A. M., Armstrong, R. S., Lay, P. A., Gow, A. J., Weiss, M. J., Mackay, J. P., and Shi, Y. (2004) *Cell* **119,** 629–640
6. Kong, Y., Zhou, S., Kihm, A. J., Katein, A. M., Yu, X., Gell, D. A., Mackay, J. P., Adachi, K., Foster-Brown, L., Louden, C. S., Gow, A. J., and Weiss, M. J. (2004) *J. Clin. Invest.* **114,** 1457–1466
7. Alayash, A. I. (2004) *Nat. Rev. Drug Discov.* **3,** 152–159
8. Rifkind, J. M., Nagababu, E., Ramasamy, S., and Ravi, L. B. (2003) *Redox Rep.* **8,** 234–237
9. Fessas, P. (1963) *Blood* **21,** 21–32
10. Nathan, D. G., Stossel, T. B., Gunn, R. B., Zarkowsky, H. S., and Laforet, M. T. (1969) *J. Clin. Invest.* **48,** 33–41
11. Finch, C. A., and Sturgeon, P. (1957) *Blood* **12,** 64–73
12. Gabuzda, T. G., Nathan, D. G., and Gardner, F. H. (1963) *J. Clin. Invest.* **42,** 1678–1688
13. Luzzatto, L., and Notaro, R. (2002) *Nature* **417,** 703–705
14. de Sanctis, D., Pesce, A., Nardini, M., Bolognesi, M., Bocedi, A., and Ascenzi, P. (2004) *IUBMB Life* **56,** 643–651
15. Halder, P., Trent, J. T., 3rd, and Hargrove, M. S. (2007) *Proteins* **66,** 172–182
16. Dewilde, S., Kiger, L., Burmester, T., Hankeln, T., Baudin-Creuza, V., Aerts, T., Marden, M. C., Caubergs, R., and Moens, L. (2001) *J. Biol. Chem.* **276,** 38949–38955
17. Lecomte, J. T., Scott, N. L., Vu, B. C., and Falzone, C. J. (2001) *Biochemistry* **40,** 6541–6552
18. Levy, A., and Rifkind, J. M. (1985) *Biochemistry* **24,** 6050–6054
19. Peterson-Kennedy, S. E., McGourty, J. L., Kalweit, J. A., and Hoffman, B. M. (1986) *J. Am. Chem. Soc.* **108,** 1739–1746
20. Robinson, V. L., Smith, B. B., and Arnone, A. (2003) *Biochemistry* **42,** 10113–10125
21. Rachmilewitz, E. A., Peisach, J., and Blumberg, W. E. (1971) *J. Biol. Chem.* **246,** 3356–3366
22. Santiveri, C. M., Pérez-Cañadillas, J. M., Vadivelu, M. K., Allen, M. D., Rutherford, T. J., Watkins, N. A., and Bycroft, M. (2004) *J. Biol. Chem.* **279,** 34963–34970
23. Fischer, G. (2000) *Chem. Soc. Rev.* **29,** 119–127
24. Shaw, P. E. (2007) *EMBO Rep.* **8,** 40–45
25. Lu, K. P., Finn, G., Lee, T. H., and Nicholson, L. K. (2007) *Nat. Chem. Biol.* **3,** 619–629
26. Marley, J., Lu, M., and Bracken, C. (2001) *J. Biomol. NMR* **20,** 71–75
27. Clore, G. M., and Gronenborn, A. M. (1994) *Methods Enzymol.* **239,** 349–363
28. Montelione, G. T., Lyons, B. A., Emerson, S. D., and Tashiro, M. (1992) *J. Am. Chem. Soc.* **114,** 10974–10975
29. Otwinowski, Z., and Minor, W. (1997) *Methods Enzymol.* **276,** 307–326
30. Navaza, J. (2001) *Acta Crystallogr. D Biol. Crystallogr.* **57,** 1367–1372
31. Jones, T. A., Zou, J. Y., Cowan, S. W., and Kjeldgaard, M. (1991) *Acta Crystallogr. A* **47,** 110–119
32. Brünger, A. T., Adams, P. D., Clore, G. M., DeLano, W. L., Gros, P., Grosse-Kunstleve, R. W., Jiang, J. S., Kuszewski, J., Nilges, M., Pannu, N. S., Read, R. J., Rice, L. M., Simonson, T., and Warren, G. L. (1998) *Acta Crystallogr. D. Biol. Crystallogr.* **54, (Pt 5)** 905–921
33. Grathwohl, C., and Wuthrich, K. (1981) *Biopolymers* **20,** 2623–2633
34. Reimer, U., Scherer, G., Drewello, M., Kruber, S., Schutkowski, M., and Fischer, G. (1998) *J. Mol. Biol.* **279,** 449–460
35. Jakob, R. P., and Schmid, F. X. (2008) *J. Mol. Biol.* **377,** 1560–1575
36. Jakob, R. P., and Schmid, F. X. (2009) *J. Mol. Biol.* **387,** 1017–1031
37. Schubert, M., Labudde, D., Oschkinat, H., and Schmieder, P. (2002) *J. Biomol. NMR* **24,** 149–154
38. Riccio, A., Vitagliano, L., di Prisco, G., Zagari, A., and Mazzarella, L. (2002) *Proc. Natl. Acad. Sci. U.S.A.* **99,** 9801–9806
39. Pesce, A., De Sanctis, D., Nardini, M., Dewilde, S., Moens, L., Hankeln, T., Burmester, T., Ascenzi, P., and Bolognesi, M. (2004) *IUBMB Life* **56,** 657–664
40. Sadelain, M., Boulad, F., Galanello, R., Giardina, P., Locatelli, F., Maggio, A., Rivella, S., Riviere, I., and Tisdale, J. (2007) *Hum. Gene. Ther.* **18,** 1–9
41. Hamdane, D., Vasseur-Godbillon, C., Baudin-Creuza, V., Hoa, G. H., and Marden, M. C. (2007) *J. Biol. Chem.* **282,** 6398–6404
42. Zhou, S., Olson, J. S., Fabian, M., Weiss, M. J., and Gow, A. J. (2006) *J. Biol. Chem.* **281,** 32611–32618
43. Brantley, R. E., Jr., Smerdon, S. J., Wilkinson, A. J., Singleton, E. W., and Olson, J. S. (1993) *J. Biol. Chem.* **268,** 6995–7010
44. Balagopalakrishna, C., Manoharan, P. T., Abugo, O. O., and Rifkind, J. M. (1996) *Biochemistry* **35,** 6393–6398
45. Dou, Y., Admiraal, S. J., Ikeda-Saito, M., Krzywda, S., Wilkinson, A. J., Li, T., Olson, J. S., Prince, R. C., Pickering, I. J., and George, G. N. (1995) *J. Biol. Chem.* **270,** 15993–16001
46. Carrell, R. W. (1999) *Science.* **285,** 1861
47. Mulcair, M. D., Schaeffer, P. M., Oakley, A. J., Cross, H. F., Neylon, C., Hill, T. M., and Dixon, N. E. (2006) *Cell* **125,** 1309–1319
48. Fothergill, J. (1982) *Nature* **298,** 705–706
49. Seidman, J. G., and Seidman, C. (2002) *J. Clin. Invest.* **109,** 451–455
50. Wedemeyer, W. J., Welker, E., and Scheraga, H. A. (2002) *Biochemistry* **41,** 14637–14644
51. Bauer, F., and Sticht, H. (2007) *FEBS Lett.* **581,** 1555–1560
52. Russell, B. S., Zhong, L., Bigotti, M. G., Cutruzzolà, F., and Bren, K. L. (2003) *J. Biol. Inorg. Chem.* **8,** 156–166
53. Shan, L., Tong, Y., Xie, T., Wang, M., and Wang, J. (2007) *Biochemistry* **46,** 11504–11513
54. Krieger, F., Möglich, A., and Kiefhaber, T. (2005) *J. Am Chem. Soc.* **127,** 3346–3352
55. Kabsch, W., and Sander, C. (1983) *Biopolymers* **22,** 2577–2637
56. Pahlke, D., Freund, C., Leitner, D., and Labudde, D. (2005) *BMC Struct.*

Biol. **5,** 8
57. Nathaniel, C., Wallace, L. A., Burke, J., and Dirr, H. W. (2003) *Biochem. J.* **372,** 241–246
58. Schultz, D. A., and Baldwin, R. L. (1992) *Protein Sci.* **1,** 910–916
59. Schultz, D. A., Friedman, A. M., White, M. A., and Fox, R. O. (2005) *Protein Sci.* **14,** 2862–2870
60. Kadokura, H., Nichols, L., 2nd, and Beckwith, J. (2005) *J. Bacteriol.* **187,** 1519–1522
61. Kadokura, H., Tian, H., Zander, T., Bardwell, J. C., and Beckwith, J. (2004) *Science* **303,** 534–537
62. McHarg, J., Kelly, S. M., Price, N. C., Cooper, A., and Littlechild, J. A. (1999) *Eur. J. Biochem.* **259,** 939–945
63. Nam, G. H., Cha, S. S., Yun, Y. S., Oh, Y. H., Hong, B. H., Lee, H. S., and Choi, K. Y. (2003) *Biochem. J.* **375,** 297–305
64. Smith, C. A., Cross, J. A., Bognar, A. L., and Sun, X. (2006) *Acta Crystallogr. D. Biol. Crystallogr.* **62,** 548–558
65. Su, D., Berndt, C., Fomenko, D. E., Holmgren, A., and Gladyshev, V. N. (2007) *Biochemistry* **46,** 6903–6910
66. Bacik, J. P., and Hazes, B. (2007) *J. Mol. Biol.* **365,** 1545–1558
67. Noble, C. G., Hollingworth, D., Martin, S. R., Ennis-Adeniran, V., Smerdon, S. J., Kelly, G., Taylor, I. A., and Ramos, A. (2005) *Nat. Struct. Mol. Biol.* **12,** 144–151
68. Ouyang, N., Gao, Y. G., Hu, H. Y., and Xia, Z. X. (2006) *Proteins* **65,** 1021–1031
69. Paoli, M., Liddington, R., Tame, J., Wilkinson, A., and Dodson, G. (1996) *J. Mol. Biol.* **256,** 775–792